Examining the effect of hydraulic turbulence in a rapid mixer on turbidity removal with CFD simulation and PIV analysis

No-Suk Park, Heekyung Park and Jong-Sub Kim

ABSTRACT

In order to investigate the effect of mixer shape and mixing intensity on hydraulic turbulence and velocity field in a rapid mixer, and relate the results of the investigation to the performance of the rapid mixer with respect to coagulant dispersion and turbidity removal, this study conducted wet tests, CFD simulation and PIV analysis, using three different shapes of jar: a circular jar with squared baffles, a circular jar without baffles and a Hudson jar. From the results of the wet tests, it was observed that the performance of rapid mixing in the circular jar without baffles was better than in the other shapes of jar. Also, the shape of jar is found to be a factor affecting the performance of the rapid mixer and ultimately the efficiency of coagulation. The results of CFD simulation and PIV analysis confirmed this by showing that, since it forms moderate turbulence throughout the jar and minimizes localized dead zones, the circular jar without baffles produced the best mixing conditions among the jars. From all these results, this study concludes that turbulent fluid conditions in a rapid mixer, including distribution of turbulence and formation of dead zones, are important factors in determining performance of the rapid mixer. Furthermore, it is suggested that mixing intensity and mixer shape are determined considering those fluid conditions.

Key words | CFD (Computational Fluid Dynamics), hydraulic turbulence, performance of rapid mixer, PIV (Particle Image Velocimetry)

No-Suk Park
Heekyung Park (corresponding author)
Department of Civil Engineering,
Korea Advanced Institute of Science and Technology (KAIST),
373-1, Kusong-dong,
Yusong-gu, Taejon,
305-701,
Republic of Korea
Tel: +82-42-869-3620
Fax: +82-42-869-3610
E-mail: *hkpark@kaist.ac.kr*

Jong-Sub Kim
Division of Civil, Environmental and Urban Engineering,
Hanbat National University,
San 16-1, Dukmyung-dong,
Yusong-gu, Taejon,
305-719,
Republic of Korea

INTRODUCTION

Rapid mixing in water treatment is used to rapidly disperse coagulant in raw water, followed by flocculation and filtration. This process has a strong influence on the overall treatment efficiency. Since the hydrolysis products, $Me_l(OH)_m^{n+}$ (Me: metal ions, OH: hydroxide ion, l,m,n: constants), of the coagulants such as alum or Fe(III) are produced within a very short time of 10^{-4} to 1 sec, and since aluminum hydroxide starts to precipitate in about 7 sec (Amirtharajah & Mills 1982), it is important to make the metallic coagulants disperse rapidly into the whole fluid bulk. However, it is practically impossible to disperse them within a second and thus it is recommended in many related publications on operation and design to disperse them as rapidly as possible (Hudson & Wolfner 1967; Vrale & Jorden 1971). In addition, since the mechanical mixing devices cannot disperse coagulants within such a short time, most operators increase the amount of coagulant determined in the laboratory by about 30–40%. This is to achieve the required efficiency of coagulation just by increasing collision opportunities between coagulant ions and colloidal particles (Kawamura 1991).

Many researchers and operators have studied a number of rapid mix parameters, including mixing intensity, time, impeller and mixer shape, coagulant dose, pH and alkalinity, as being important for the whole operation of the coagulation and flocculation process. Among them, the physical parameters such as mixing intensity and retention time are known to be more important than the chemical parameters such as pH and

alkalinity of water to be treated (Mhaisalkar *et al.* 1991). The mixing intensity is usually represented in terms of power input or velocity gradient, G, and the mixing time is defined as retention time in the mixer after coagulant injection. After the G value was introduced as an index representing mixing intensity, Camp suggested that the product of $G \cdot t$, where G = mean velocity gradient and t = retention time, should be used as the main parameter for the operation and design of the mixer (Gorden 1991). Bratby suggested design values of velocity gradient and mixing time of 650 sec^{-1} and 0.5–8 sec, respectively, for a raw water with turbidity of 140 NTU (Bratby 1981). Ghosh *et al.* (1985) suggested an optimal velocity gradient of 800 sec^{-1} for a raw water of 25 NTU. They conducted experiments for a fixed mixing time of 120 sec (Ghosh *et al.* 1985). However, as discussed in *Water Quality and Treatment* (AWWA 1990), there are no clear-cut guidelines for determining power dissipation or mixing time required to disperse coagulant. Also, Lai *et al.* (1975) pointed out the inadequacy of the use of $G \cdot t$, showing that different combinations of G and t, even though their product values are identical, can yield very different results in coagulation and flocculation.

As can be seen in these previous works, there are some conflicts in recommendations in literature on velocity gradient and mixing time. We think some of the reasons for the conflicts are as follows. First, the properties of the raw water used were not identical. Secondly, since the geometries of mixers and impellers used in the experiments were not identical, the properties of hydraulic turbulence were not the same. Lastly, either mixing time or velocity gradient has been varied during the experiments. Since the fixed parameter is not identical in most of the previous investigations, the results cannot be compared (Mhaisalkar *et al.* 1991).

Coagulant dispersion depends strongly on the properties of hydraulic turbulence and the spatial velocity distribution, i.e. velocity gradients from point to point in a mixer (Oldsue 1983). Also, the properties of hydraulic turbulence and the spatial velocity distribution depend on the pattern of energy dissipation, even with the same amount of mechanical energy being supplied, which is inevitably related to the types of mixer used. However, only a few studies have been carried out on them in a rapid mixer. Amirtharajah showed that the chemical reactions between coagulant ions and colloidal particles depend on the turbulent fluid conditions in rapid mixers and emphasized the importance of the interactions between them (Amirtharajah & Mills 1982). Mhaisalkar *et al.* (1991) examined the effect of mixer shape on flocculation using drag force on the rotating impeller and concluded that the existence of baffles in a mixer, and a hexahedron shape of mixer, both help increase mixing intensity. Nagata (1975) studied an eight-blade radial-flow turbine over a wide range of Reynolds number in a mixer, trying to quantify flow and power number, and found that the ratio of inertia force to viscous force governs flow and power number over a wide range of Reynolds number in a mixer.

Recognizing the significance of hydraulic turbulence in a rapid mixer, and the need to investigate it more thoroughly, this study analyses, in depth, turbulent fluids in three different types of mixer at different G values, using computational fluid dynamics (CFD) simulations and particle image velocimetry (PIV) techniques. We also conducted wet tests using those mixers and the same G values. From the wet tests, CFD and PIV results, we discuss hydraulic turbulence in a mixer and its effects on mixing.

MATERIAL AND METHODS

Wet tests

Wet tests were carried out with three different types of acrylic jar shown in Figure 1. A kaolin dispersion of 2 litres (l) was used for each test and its initial turbidity was 5.70 NTU. In *Water Treatment Plant Design and Operation* (AWWA 1998) it is stated that 'no standard design exists' for jars or jar-test apparatus. Currently, square baffled vessels and Hudson jars are widely used. As shown in Figure 1, we used three types of jar for our study: a circular jar with squared-baffles, a circular jar with no baffles and a Hudson jar with no baffles. The first circular square-baffled jar has four baffles. The baffles, each one-tenth of the vessel diameter in width, are positioned symmetrically on the vessel wall, forming vertically

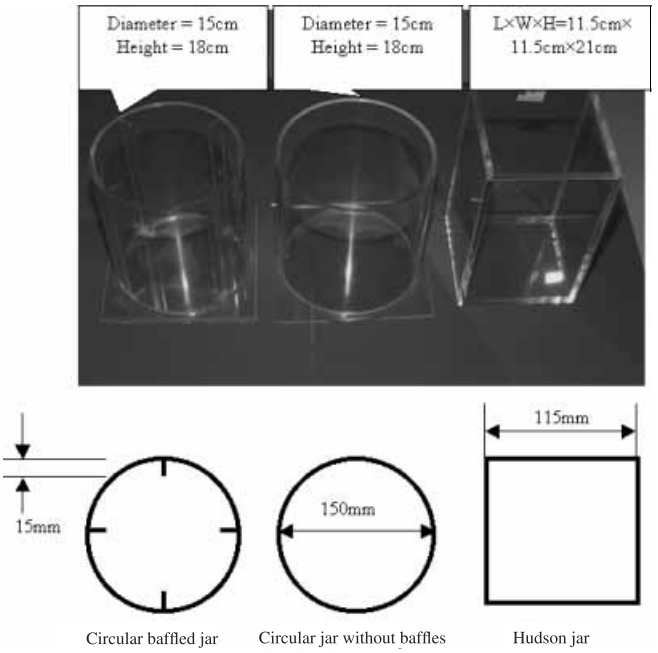

Figure 1 | Three different types of jar used in the wet tests.

mounted radial strips. The diameter of the vessels is 150 mm. The second circular jar is exactly same shape as the first jar except that there are no baffles. The third, Hudson, jar is a hexahedron vessel and has no baffles. It is 115 mm in both length and width and 210 mm in height.

A stainless steel impeller with two flat blades was used for these tests. This impeller consists of two vertically mounted blades and a rotating vertical shaft. The inner and outer radii of the blades are 3 mm and 38.1 mm, respectively. The width of the blades is 15 mm. Since the blade is set at half the depth of the water in each jar, in the cases of the circular baffled jar and the jar without baffles the centre of the impeller is located at a height of 6 cm from the vessel bottom, while in the case of the Hudson jar, it is about 8 cm from the bottom.

Since the main objective of this study is to investigate the influence of hydraulic turbulence in rapid mixers on coagulation, dispersion and turbidity removal, chemical parameters are set to keep constant as far as possible. Kaolin dispersion for the test was achieved by mixing kaolin with distilled water and adding 2 meq/l of sodium bicarbonate for alkalinity (Andreu-Villegas & Letterman 1976). Then the pH was adjusted with acetic acid to an optimal pH value of 7.1 after the addition of coagulant (Gorden 1991). We chose kaolin, because it has been shown or proved that its results are similar to those of the turbidity materials in the natural raw water (McCooke & West 1978).

The details of the procedure are summarized as follows. We first weighed approximately 5 g of kaolin, dried it at 105°C, and mixed it with 150 ml of distilled water. Then the mixture was left for 24 h. Distilled water was added to make it up to 200 ml, followed by blending at 6,000 rpm for 3 min. Again, distilled water was added to make it up to 800 ml and blended. The 800 ml solution was kept unshaken for 24 h for the precipitate to settle. Approximately 600 ml of that solution was then decanted to make a stock solution and was mixed with $NaHCO_3$, which was then dried at 105°C for 90 min, to make a $NaHCO_3$ stock solution of 16.8 g/l (Gorden 1991). This stock solution was maintained at 1% strength and made fresh every week, as recommended by Tekkipe & Ham (1970).

The procedure of the wet tests was as follows. Sample water for each test was made by mixing 1,900 ml of distilled water, 80 ml of kaolin stock suspension, 20 ml of sodium bicarbonate, and 3 ml of acetic acid (5% v/v). Turbidity in all tests was measured in NTU with the HACH 2100N turbidimeter, which has an accuracy of 0.01 NTU. A rapid mixing time of 15 sec was chosen to limit any possibility of flocculation, as the conventional jar test procedure suggests 15–60 sec for rapid mixing (Purchas 1977; AWWA 1998). Hudson & Wolfner (1967) recommend mixing coagulant with the bulk in as short a time as possible. After rapid mixing, the impeller rotating speed was set at 50 rpm for 15 min. After 10 min settling time, a sample of approximately 20 ml was taken from 20 mm below the surface for measurement. The optimal pH and coagulant dose for turbidity removal with aluminium sulphate ($Al_2[SO_4]_3 \cdot 18H_2O$) for kaolin dispersion, which were determined by this procedure, were 7.1 and 5 ppm, respectively. These values were applied for all tests. To evaluate the degree of charge neutralization for destabilization and the efficiency of coagulant dispersion, the zeta potential was measured with a Model No. 2100 Malvern Zetasizer immediately after 10 sec of rapid mixing. Kawamura (1991) has emphasized that as the zeta

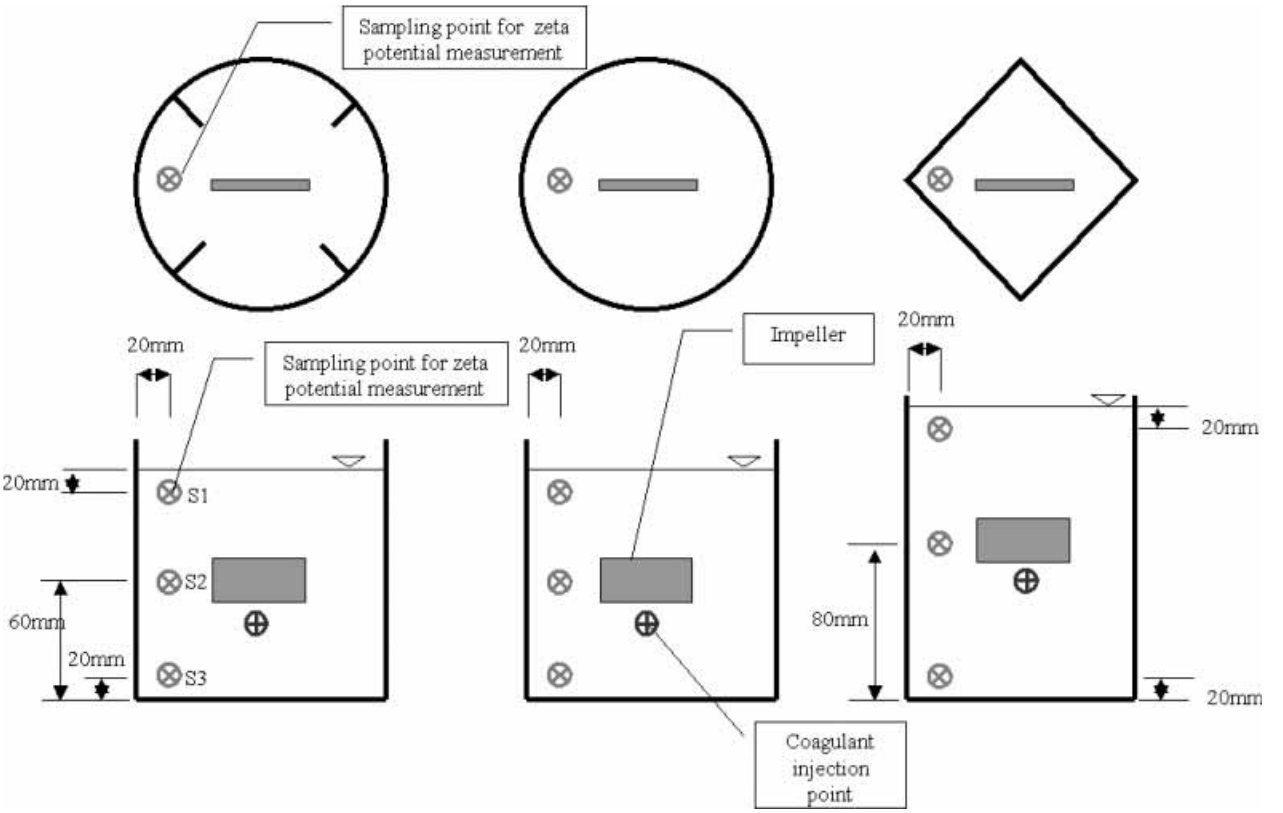

Figure 2 | Schematic for zeta potential measurement and coagulant dose.

potential of floc seed in bulk becomes closer to absolute 0 mV, the efficiency of the following coagulation-flocculation process becomes higher. This indicates that zeta potential can be an index with which coagulant dispersion and coagulation efficiency can be evaluated. Samples were taken at three points using syringes after the 10 sec of rapid mixing. As shown in Figure 2, they are located at 20 mm below the surface, at the height of the rotating impeller and 20 mm above the bottom. Coagulant was injected just beneath the impeller (see Figure 2), as suggested by Mhaisalkar *et al.* (1991), to ensure uniform dispersion of coagulant in the mixer.

As shown in Table 1, each shape of mixer was tested at 12 different impeller speeds. The G values in different types of mixer are different from each other at the same impeller speeds, as shown. This is because G values are calculated from voltages and electrical currents measured by a tachometer.

Methodology of CFD simulation

Governing equations

To investigate the relationship between turbulent fluid and coagulant dispersion in a mixer, which can be extended to explain the results of wet tests, velocity field and energy dissipation in each jar were simulated using CFX4.2 which was developed by AEA technology (AEA Technology 1995). The CFD simulation works by splitting the geometry of interest into a large number of elements, collectively known as 'grids' or 'cells'. Then, momentum and continuity equations are formulated for each grid together with given boundary conditions, and then repeatedly solved by using FVM (Finite Volume Method). The time-averaged Navier-Stokes equations for momentum and continuity were solved in this study for steady, incompressible, turbulent and isothermal flow.

The continuity and momentum equations are, respectively:

Table 1 | Experimental matrix for wet tests

Impeller speed (rpm)	*G* value (sec^{-1}) Circular baffled jar	Circular jar without baffles	Hudson jar	Initial turbidity (NTU)	Conditions
125	81.8	48.6	129.4	5.70 NTU	—Rapid mixing time: 15 sec —Slow mixing time: 15 min —Coagulation dose: 5 ppm
150	100.2	60.0	147.8		
175	119.0	71.6	165.4		
200	131.7	83.5	182.3		
225	157.4	95.7	198.6		
250	177.0	108.1	214.5		
275	196.9	120.6	229.9		
300	216.9	133.4	244.9		
325	237.1	146.3	259.6		
350	257.5	159.3	274.0		
375	278.1	172.5	288.2		
400	298.8	185.9	302.0		

$$\underline{\nabla} \cdot (\underline{U}) = 0 \tag{1}$$

$$\underline{\nabla} \cdot (\rho \underline{U} \otimes \underline{U} - \mu \underline{\nabla U}) = \underline{B} + \underline{\nabla} P - \underline{\nabla} \cdot (\overline{\rho \underline{u} \otimes \underline{u}}) \tag{2}$$

where ρ and μ are fluid density and dynamic viscosity, respectively; P is pressure; $\underline{U}$ the fluid mean velocity; $\underline{B}$ a body force; and $\underline{u}$ the fluctuating velocity.

Impeller modelling

The momentum sources representing the effect of the impeller are derived from a balance of the torque acting on the impeller and the shaft. The torque was calculated by integrating over the volume swept by the impeller, V_s, the azimuthal reaction force of the fluid on the impeller, F, multiplied by the radius of action, r. It is:

$$T = \int_{V_s} rF dV \tag{3}$$

where T is the impeller torque.

This volumetric force is a time-averaged one, neglecting the periodic fluctuations in the flow generated by rotation of two blades. The force was assumed to be uniform in the circumferential and axial direction, and to be proportional to a radial distance, as shown in Equation (4):

$$F = Kr \tag{4}$$

where K is the volumetric force divided by a radial distance.

Substituting Equation (4) into Equation (3) results in:

$$T = \int_{r_1}^{r_2} 2\pi r^3 KW dr \tag{5}$$

where W is the axial depth of the impeller, and r_1 and r_2 are respectively the inner and outer radii of the impeller. The integration of Equation (5) leads to the value of K as shown in Equation (6).

$$K = \frac{2T}{\pi w[r_2^4 - r_1^4]} \tag{6}$$

In the simulations of this study, the axial depth of the impeller, W, is 15 mm and the radius of blade, r_2, is 38.1 mm. The radius of shaft, r_1, is assumed to be 0 mm, though it is in fact 3 mm, just for simplicity. This volumetric force acts in the circumferential direction in each of the cells within the impeller region. The momentum equations represent the conservation of momentum in the Cartesian x, y and z directions. Since the volumetric force must be projected into these directions within the impeller volume, the x, y and z components of the force are expressed as shown in Equation (7), (8) and (9).

$$F_x = -\frac{Fy}{\sqrt{x^2 + y^2}} \tag{7}$$

$$F_y = -\frac{Fx}{\sqrt{x^2 + y^2}} \tag{8}$$

$$F_z = -F \tag{9}$$

These components of the force are implemented in their relevant momentum equations as source per unit volume. Also, the body force vector, $\underline{B}$, is expressed as shown in Equation (10):

$$\underline{B} = \left(\frac{F_x}{V}, \frac{F_y}{V}, \frac{F_z}{V} \right) \tag{10}$$

where V is the volume of each cell.

Turbulence modelling

Since the Reynolds number of the impeller is high enough to guarantee turbulent fluid conditions in a jar, all cases were simulated by turbulent modelling (Perry & Chilton 1973). The turbulence in each jar is significantly anisotropic due to the rotation which generates circumferentially stretched turbulent eddies. Therefore, a differential Reynolds-stress model was used for modelling the turbulence transport of momentum. The transport equations were solved for obtaining the turbulent stresses and the turbulence energy dissipation rate.

Boundary conditions

The liquid free surface at the top is considered flat and frictionless, i.e. as a symmetry plane, even if there are some fluctuations at the surface due to the rotation of the impeller. This is because the fluctuations are usually small enough to be neglected for the purposes of this study. At the vessel wall and the baffle surface, a no-slip condition was assumed, and the well-known wall-function method was used to bridge the viscous sub-layer. Therefore, it is assumed that each component's velocity at the vessel wall and the baffles is zero. The wall shear stress was obtained from the logarithmic law of the wall (Currie 1993). In addition, a water temperature of 20°C was selected from the measurement, and the differential turbulence model was specified.

Methodology of PIV analysis

The PIV system has been developed as a quantitative flow visualization device. It uses an optical imaging technique to measure velocities simultaneously at many points in a flow field (Adrian 1986; Rajengran & Patel 2000). A laser sheet, generated by expanding a laser beam with a combination of cylindrical and spherical lenses, illuminates a planar flow region. Seeding particles must be sufficiently small and non-buoyant to follow fluid motion (Adrian 1986). This study selected PVC (poly-vinyl chloride) as a seeding particle since it has a similar density (1.05 g/ml) to water, which is desirable in relating the particle motion to the water velocity. The motion of the seeding particle is then captured by a recording device, such as a CCD (charge-coupled device) camera. As shown in Figure 3, the PIV system used in this study consisted of an Argon laser, a high speed CCD camera, lenses, a controller, a host computer (Pentium III 650 MHz) and PIV software. The PIV software used an auto-correlation technique to find the displacement of particles before plotting the vectors in a uniform grid (Rajengran & Patel 2000). An interrogation area of 362×362 pixels was chosen and the velocity vectors were plotted on the image in a 40×30 grid. The relative positions of the viewing area in each jar were side planar including impeller shaft, and 60 consecutive images were recorded at an interval of 1 sec. The results of the PIV analysis were compared with those of the CFD simulation later.

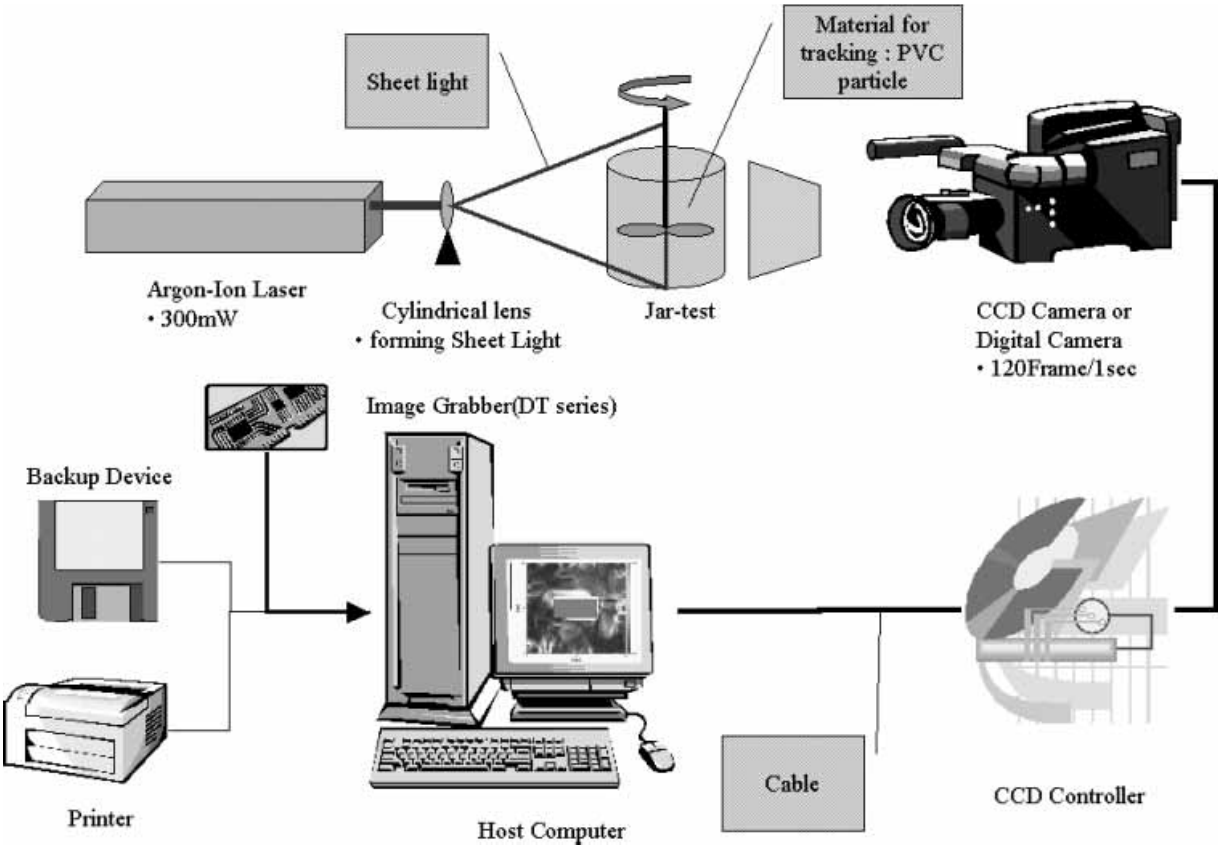

Figure 3 | Schematic of the PIV system used in this study.

RESULTS AND DISCUSSION

Results of wet tests

Figure 4 shows the zeta potentials measured at various rotating speeds in each jar immediately after 10 sec of rapid mixing. The initial zeta potential of kaolin dispersion, just before the rapid mixing, was -55.0 mV. As shown in Figure 4, at S1, which is 20 mm below the surface in each jar, the zeta potential first increases and then becomes almost constant, as the rotating speed increases. At S2, in the vicinity of the impeller, the zeta potential values are close to 0 mV from the beginning and become closer to it as the rotational speed increases. On the other hand, at S3, which is 20 mm above the bottom of the jar, the zeta potential first decreases and then becomes almost constant as the rotating speed increases. Considering that a zeta potential close to absolute 0 mV is better for coagulation-flocculation, as discussed by Kawamura (1991), the results indicate that the efficiency of mixing is the highest in the vicinity of S2, and that the poor efficiencies in the regions of S1 and S3 improve as the rotating speed increases to the turning speed, and stay almost constant as it increases further. The turning rotating speeds over which the zeta potential becomes stabilized are about 200 rpm in the circular baffled jar, 250 rpm in the circular jar without baffles and 150 rpm in the Hudson jar, as shown in Figure 4. These can be explained by the following two factors. First, since coagulant is injected in the vicinity of the low edge of the impeller, many of the reactions that $Al_l(OH)_m^{n+}$ forms in a second through hydrolysis of the coagulant and then combination with the colloids nearby, occur in the region below the impeller. That is why the zeta potential in S2 is

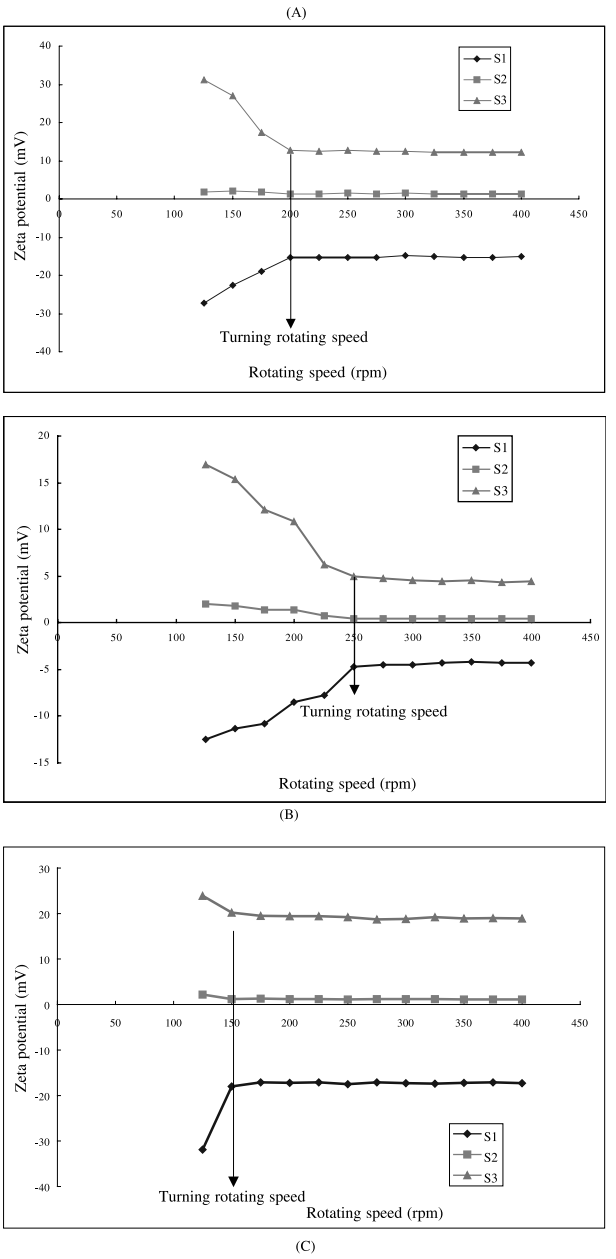

Figure 4 | Zeta potentials (mV) measured immediately after 10 sec of rapid mixing: (A) circular baffled jar, (B) circular jar without baffles, (C) Hudson jar.

much closer to 0 mV. The second factor is that before the alum coagulant reaches the free surface and the bottom of the jar, it is converted into hydroxo-aluminium complexes, $Al(OH)_3(s)$, since this conversion takes only 10^{-4}–1 sec.

Table 2 | Comparison of zeta potentials measured at the three sampling points

Sampling points	Circular baffled jar (mV)	Circular jar without baffles (mV)	Hudson jar (mV)
S1	– 15.4	– 4.7	– 18.0
S2	1.4	0.5	1.2
S3	12.7	5.0	20.2
Difference between S1 and S3	28.1	9.7	38.2

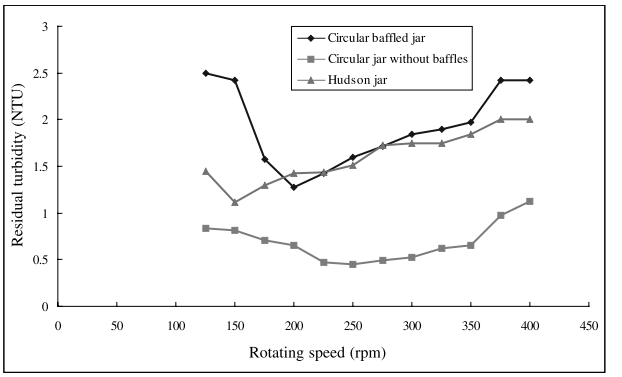

Figure 5 | Comparison of residual turbidity (NTU).

As summarized in Table 2, the differences between S1 and S3 at the turning rotating speeds are 28.1 mV in the circular baffled jar, 9.7 mV in the circular jar without baffles and 38.2 mV in the Hudson jar. This shows that the circular jar without baffles has the smallest difference. In addition, the zeta potential at S2 in the circular jar without baffles is 0.5 mV, and closer to 0 mV than the other cases. These results indicate that the mixing conditions in the circular jar without baffles disperse the coagulant more efficiently than those in the other jars, and thus provide much better conditions for coagulation.

Figure 5 shows residual turbidities (NTU) in the three jars. In the circular jar without baffles, a residual turbidity of 0.45 NTU is the lowest at a rotating speed of 250 rpm at which the G value is 108.1 s^{-1}. (They are called here the optimum rotating speed and G value, respectively.) As the rotating speed and G value further increase, the residual turbidity also increases. In the circular baffled jar, the

optimum rotating speed and G value are 200 rpm and 131.7 s^{-1}, respectively, at which the residual turbidity is 1.28 NTU. In the Hudson jar, they are 150 rpm and 147 s^{-1} with a residual turbidity of 1.11 NTU. (As previously mentioned, the initial turbidity of kaolin dispersion is 5.70 NTU.) Interestingly, it is noted that the optimum rotating speeds and G values in different jars are not identical, and that the turning rotating speed discussed above with zeta potential and the optimum rotating speed in each jar are identical. This indicates that the shape of the jar and the presence of baffles can affect the optimum mixing conditions. Also, the turning rotating speed over which the zeta potential becomes stabilized can be the optimum mixing condition under which residual turbidity is lowest, based on the charge neutralization-destabilization mechanism.

The residual turbidity at the optimum G value is the lowest in the circular jar without baffles, and the highest in the circular baffled jar. In addition, the optimum G value in the circular jar without baffles is the lowest, at 108.1 s^{-1}. This indicates that the baffles in a mixer and a hexahedron shape do not improve the dispersal of coagulant at all and, ultimately, the turbidity removal. This result is a good match with what Oldsue (1983) emphasized. He said that in the case of mixing fluids of low viscosity, baffles in a mixer increase power consumption by the impeller but rather decrease the overall general motion of fluid in the mixer. In particular, he discussed the 'overbaffling phenomenon'. That is, even if they tend to prevent vortex formation at the free surface at high rotating speed, the baffles may reduce mass flow and localize the mixing, and eventually cause poor performance (Oldsue 1983). Our test results exactly confirm his observations. The G value, which represents the energy consumption, is lower in the circular jar without baffles than in the other two jars, however, mixing performance in terms of turbidity removal, is the best in the circular jar without baffles (refer to Table 1 and Figure 5).

Results of CFD simulation and PIV analysis

As observed in the results of zeta potential and residual turbidity shown and discussed above, the circular jar without baffles yields the smallest difference of zeta potential between the three measuring points and the lowest residual turbidity at the optimum G value. This indicates that shape of jar and presence of baffles in the jar can affect the efficiency of coagulation and flocculation and that the circular jar without baffles is better for mixing than the other two types of jar. Also, the results confirm what Mhaisalkar *et al*. (1991) and Gorden (1991) discussed, that the G value and rotating speed over their optimum values rather increase the residual turbidity. That is, the results illustrate that extra energy supplied over a certain intensity, i.e. a turning rotating speed, may be used for breaking flocs rather than diffusing coagulant. We think the turbulent fluid condition in the mixer produces these results. To confirm this result, we simulated the turbulences in each jar and developed images of its turbulence fields in depth, using CFD technique and PIV analysis, respectively. Then we related these results to the wet test results discussed above.

The dissipation of supplied energy and turbulence created in an individual jar at its optimum G value (i.e. its optimum rotating speed) are simulated with CFD software and also analysed with the PIV system. Figure 6 shows the results of the CFD simulation and the 2-D PIV analysis in the left-and right-hand columns, respectively. Both of them show the contour of absolute value of velocity in each case. The circular baffled jar at a G value of 131.7 s^{-1} is shown in (A), the circular jar without baffles at a G value of 108.1 s^{-1} in (B), and the Hudson jar at a G value of 147.8 s^{-1} in (C).

For comparison, first of all, we must note that the CFD simulation was done in three dimensions while the PIV analysis took an image of velocity in two dimensions. First, we can compare a key that represents a range of velocity with the highest and the lowest. For the circular baffled jar, the highest velocity of the CFD simulation is 0.200 m/sec while that of the PIV analysis is 0.186 m/sec. For the circular jar without baffles, they are 0.137 m/sec and 0.109 m/sec, respectively and for the Hudson jar, they are 0.277 m/sec and 0.269 m/sec, respectively. As noted, the velocities measured by the PIV analysis were a little lower than those of the CFD simulation. Since a velocity in two dimensions is a projection of it in three dimensions, the former must be a little lower than the latter. As a

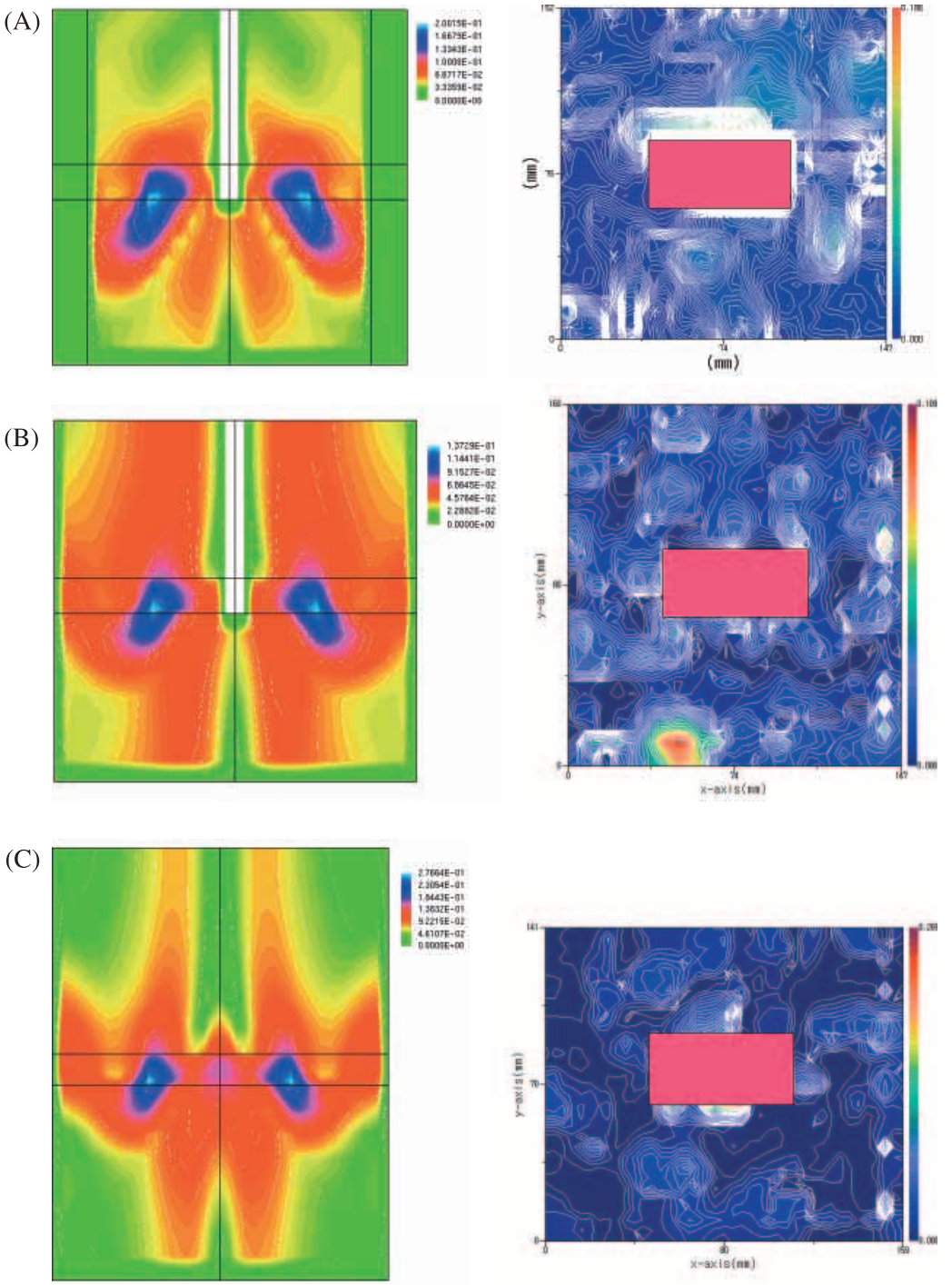

Figure 6 | Contour of absolute value of velocity from results of CFD simulation (left column) and PIV analysis (right column): (A) circular baffled jar, (B) circular jar without baffles, (C) Hudson jar.

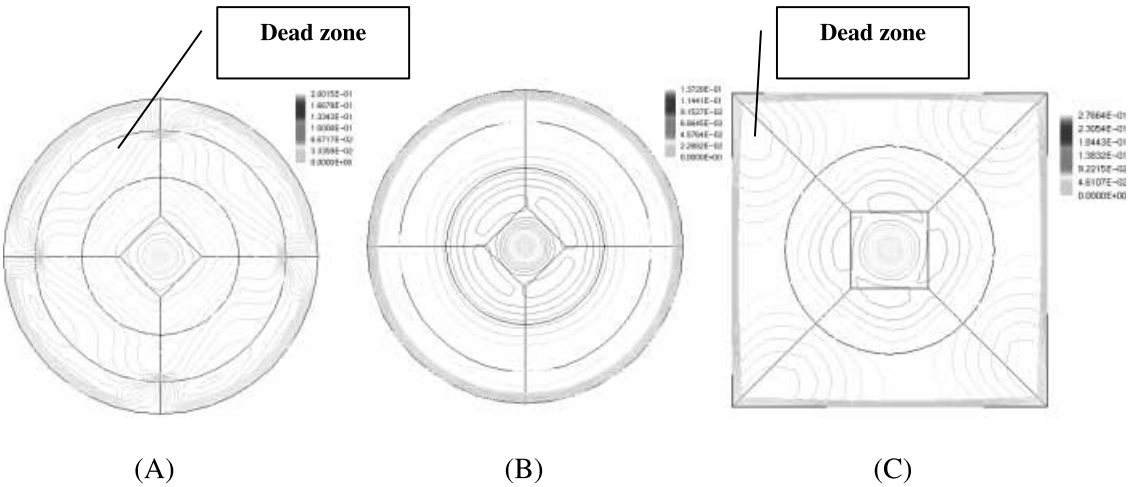

Figure 7 | Formation of dead zones from the results of CFD simulation: (A) circular baffled jar, (B) circular jar without baffles, (C) Hudson jar.

result, we think the differences are generated from the dimensional difference and conclude that both results are a good match and verify each other fairly well.

Secondly, we can think of the pattern of energy dissipation and the distribution of turbulence generated from energy dissipation. The supplied mechanical energy through the shafts and impellers is converted into velocity energy in mixers. In the results of the CFD simulation, the blue and green lines in each case represent velocities higher than 66% of the highest velocity and velocities lower than 33% of the highest velocity, respectively (note that the highest velocities in individual jars are different). The red lines are in the middle of the range. It can be said from this classification that the blue and red lines represent relatively high turbulence in each case. It is also noted that in the circular jar without baffles, the red lines are distributed from the top to the bottom with a concentration at the centre. On the other hand, in the cases of (A) and (C), the green lines are distributed widely and the red ones are concentrated in the region of impeller and along the baffles and walls. In all cases, blue lines are concentrated only in the vicinity of impeller blades. This indicates that the supplied energy is dissipated throughout the volume of the jar in the case of (B), creating more mass flows in it, but not in the cases of (A) and (C). As a result, the turbulent fluid conditions in the jar of case (B) are better for mixing than those in the other two jars.

The results of PIV analysis confirm these findings. The white areas represent rapid transformation of velocities from point to point in each recorded image. Due to limitations in resolution of those images, the region where velocity contours are concentrated densely is represented by white colour. Therefore, a more even distribution of the white coloured areas throughout a section means that the supplied energy is dissipated more evenly, and that steep local velocity gradients, which promote better mixing performance, occur more efficiently in this section (Park & Park 2001). As shown, the white coloured areas are better distributed in the case of (B) than in the cases of (A) and (C), which means that the case of (B) is better than those of (A) and (C), when being compared in terms of the distribution of steep local velocity gradients in a jar. This result is in accordance with that of the CFD simulation.

Thirdly, we have to look at the formation of dead zones. Figure 7 shows contours of absolute value of velocity from horizontal sectional views of the jars at a height of 0.02 m from the bottom. As shown, dead zones are generated around the corners in the Hudson jar and in the vicinity of the baffles in the circular baffled jar. However, dead zones are not clearly observed in the circular jar without baffles. Generally speaking, such formation of dead zones will inhibit dispersal of coagulant.

The results are summarized in Table 3 in terms of distribution of turbulence, the pattern of energy

Table 3 | Comparison of the results of CFD simulation and PIV analysis

Types	Circular baffled jar	Circular jar without baffles	Hudson jar
CFD simulation			
Distribution of turbulence	In the regions of rotating impeller, side walls and baffles	Throughout the jar	In the regions of rotating impeller and sidewalls
Pattern of energy dissipation	Localizes the dissipation of input energy on impeller and baffles	Dissipates the input energy throughout its volume	Localizes the dissipation of input energy on impeller and sidewalls
Formation of dead zones	Observed in the vicinity of baffles	Not observed	Observed in each corner
Highest velocity	0.200 m/sec	0.137 m/sec	0.277 m/sec
PIV simulation			
Distribution of turbulence	In the region of rotating impeller	Throughout the jar	In the region of rotating impeller
Pattern of energy dissipation	Localizes the dissipation of input energy on impeller	Dissipates the input energy throughout its volume	Localizes the dissipation of input energy on impeller
Highest velocity	0.186 m/sec	0.109 m/sec	0.269 m/sec

dissipation, the formation of dead zones and the highest velocities. All of these results indicate that the overall mixing efficiency in the circular jar without baffles is the best of the three jar types, and that baffles and hexahedron shapes may increase the formation of dead zones, reduce the overall mass flow, localize mixing and thus inhibit dispersal of coagulant. Mhaisalkar *et al.* (1991) expected baffles and hexahedron shapes to increase the drag force on the impeller blades and G values, and theoretically promote mixing efficiency and coagulant dispersion. However, the results of this study indicate that, even though baffles and a hexahedron shape increase the G value, this increase localizes fluid movement, creates dead zones and worsens mixing efficiency and coagulant dispersion, which is contrary to what Mhaisalkar *et al.* (1991) expected. The results of wet tests measured in zeta potential and residual turbidity confirm what we found in this study. Accordingly, we conclude that as long as reasonably turbulent fluid conditions are created in a jar, distribution of turbulent flow and formation of dead zones in the jar are important factors affecting the performance of mixing, coagulant dispersion and turbidity removal in water treatment.

SUMMARY

In this study, we investigated the effect of mixer shape and mixing intensity on hydraulic turbulence and velocity fields in a rapid mixer, and related the results of the investigation to the performance of a rapid mixer in terms of coagulant dispersion and turbidity removal. For this, we have conducted wet tests, CFD simulation and PIV analysis, using three different shapes of jar. The results of this study are summarized as follows:

The results of the wet tests showed that the impeller rotating speeds and G values for the most effective

turbidity removal in different shapes of jar were not identical. The residual turbidity and the optimum G value in the circular jar without baffles were the lowest, the second lowest values were in the Hudson jar and the highest values in the circular baffled jar. This suggests that different shapes of jar can affect the performance of rapid mixing and eventually the efficiency of coagulation.

Comparison of the measurements of zeta potential with those of residual turbidity (Figures 4 & 5) shows that the optimum impeller rotating speeds and G values in individual jars are almost the same as those at their zeta potential turning speeds. Considering the characteristics and required times of alum hydrolysis, and the limitations of mechanical mixing devices, this suggests that the extra mixing intensity over a zeta potential turning speed may be used for breaking flocs rather than dispersing coagulant, Also, it confirms the discussions in some of the previous research that G values above the optimum in a rapid mixer worsen turbidity removal.

The results of wet tests, CFD simulation and PIV analysis (Figure 6 and Table 3) proved that, since it forms relatively high turbulence throughout the jar and minimizes dead zones, the circular jar without baffles produced the best mixing conditions among the three jar shapes. This indicates that baffles and a hexahedron shape may not promote mixing efficiency, coagulant dispersion and ultimately turbidity removal in water treatment, even though they increase the power consumption of the impeller (included in G value as power) and the G value.

All these results indicate that turbulent fluid conditions in a rapid mixer, including distribution of turbulence and formation of dead zones, are important factors in determining the performance of a rapid mixer. Furthermore, it can be concluded that mixing intensity and mixer shape must be determined considering those fluid conditions.

This can be extended to design and operation of the rapid mixer and jar-test apparatus. As known, many researchers have recently discussed the inadequacy of the G value for such purposes (Oldsue 1983; Cleasby 1984; Clark 1985; Han & Lawler 1992). Based on the results of this study, it can be pointed out that the G value and $G{\cdot}t$ are inadequate for designing and operating rapid mixer and jar-test apparatus since they cannot reflect such important hydraulic conditions in themselves. More detailed discussion on this matter is given in Park & Park (2001).

REFERENCES

Adrian, R. J. 1986 Image shifting technique to resolve directional ambiguity in double pulsed velocimetry. *Appl. Optics* **25**(21), 3855–3858.

AEA Technology 1995 *CFX Application Manual*. AEA Technology, Oxfordshire, United Kingdom.

American Water Works Association 1990 *Water Quality and Treatment*. McGraw-Hill, New York.

American Water Works Association 1998 *Water Treatment Plant Design and Operation*. McGraw-Hill, New York.

Amirtharajah, A. & Mills, P. 1982 Rapid mix design for alum coagulation. *J. Am. Wat. Wks Assoc.* **74**(5), 210–216.

Andreu-Villegas, R. & Letterman, R. D. 1976 Optimizing flocculator power input. *J. Environ. Eng, ASCE* **102**(2), 251–263.

Bratby J. R. 1981 Interpreting laboratory results for the design of rapid mixing and flocculation systems. *J. Am. Wat. Wks Assoc.* **73**(6), 318–325.

Clark, M. M. 1985 Critique of Camp and Stein's RMS Velocity gradient. *J. Environ. Eng, ASCE* **111**(6), 741–754.

Cleasby, J. L. 1984 Is velocity gradient a valid turbulent flocculation parameters? *J. Environ. Eng. ASCE* **100(**5), 875–897.

Currie, I. G. 1993 *Fundamental Mechanics of Fluids*. McGraw-Hill, New York.

Ghosh, M. M., Cox, C. D. & Prakash, T. M. 1985 Polyelectrolyte selection for water treatment. *J. Am. Wat. Wks Assoc.* **77**(3), 67–73.

Gorden, L. M. 1991 Turbulence Intensity of Mixing Relation to Flocculation. *J. Environ. Eng. ASCE* **117**(6), 731–748.

Han, M. & Lawler, D. F. 1992 The (relative) insignificance of G value in flocculation. *J. Am. Wat. Wks Assoc.* **84**(10), 79–91.

Hudson, H. E. & Wolfner, J. P. 1967 Design of Mixing and Sedimentation Basins. *J. Am. Wat. Wks Assoc.* **59**(10), 1257–1268.

Kawamura, S. 1976 Consideration in improving flocculation. *J. Am. Wat. Wks Assoc.* **68**(5), 328–336.

Kawamura, S. 1991 *Integrated Design of Water Treatment Facilities*. John Wiley & Sons, Inc.

Lai, R. J., Hudson, H. E. & Singley, J. E. 1975 Velocity gradient calibration of jar-test equipment. *J. Am. Wat. Wks Assoc.* **67**(10), 553–557.

Letterman, R. D., Quon, J. E. & Gemmell, R. S. 1973 Influence of rapid mix parameters on flocculation. *J. Am. Wat. Wks Assoc.* **65**(11), 716–722.

McCooke, N. J. & West, J. R. 1978 The coagulation of the kaolin suspension with alum. *Wat. Res.* **12**, 793–798.

Mhaisalkar, V. A., Paramasivam, R. & Bhole, A. G. 1991 Optimizing Physical Parameters of rapid mix design for

coagulation-flocculation of turbid waters. *Wat. Res.* **25**(1), 43–52.

Nagata, S. 1975 *Mixing: Principles and Applications*. Wiley, New York.

Oldsue, J. Y. 1983 *Fluid Mixing Technology*. McGraw-Hill, New York.

Park, N. S. & Park, H. (2001) Evaluation of the adequacy of G value in rapid mixer. *J. Environ. Eng. ASCE* (submitted).

Perry, R. H. & Chilton, C. H. 1973 *Chemical Engineer's Handbook* (5th edition). McGraw-Hill, New York.

Purchas, D. B. 1977 *Solid-Liquid Separation Equipment Scale-Up*. Uplands Press, Croydon, U.K.

Rajengran, V. P. & Patel, V. C. 2000 Measurement of vortices in model pump-intake bay by PIV. *J. Hydraulic Eng. ASCE* **126**(5), 322–334.

Tekkipe, R. J. & Ham, R. K. 1970 Coagulation testing – A comparison of techniques. *J. Am. Wat. Wks Assoc.* **62**(9/10), 594–602, 620–628.

Vrale, L. & Jorden, R. M. 1971 Rapid mixing in water treatment. *J. Am. Wat. Wks Assoc.* **63**(1), 52–58.

First received 30 August 2001; accepted in revised form 10 April 2002